Eur. Phys. J. B **7**, 401–410 (1999)

THE EUROPEAN PHYSICAL JOURNAL B

EDP Sciences

Effects of finite thickness on interfacial widths in confined thin films of coexisting phases

T. Kerle[1], J. Klein[1,a], and K. Binder[2]

[1] Department of Materials and Interfaces, Weizmann Institute of Science, 76100 Rehovot, Israel
[2] Institut für Physik, Johannes Gutenberg Universität Mainz, 55099 Mainz, Germany

Received: 19 February 1998 / Received in final form: 2 September 1998 / Accepted: 8 September 1998

Abstract. The capillary broadening of a 2-phase interface is investigated both experimentally and theoretically. When a binary mixture in a thin film with thickness D segregates into two coexisting phases the interface between the two phases may form parallel to the substrate due to preferential surface attraction of one of the components. We show that the interfacial profile (of intrinsic width w_0) is broadened due to capillary waves, which lead to fluctuations, of correlation length $\xi_\parallel$ of the local interface positions in the directions parallel to the confining walls. We postulate that $\xi_\parallel$ acts as an upper cutoff for the spectrum of capillary waves on the interface, so that the effective mean square interfacial width w varies as $w^2 \propto \ln \xi_\parallel$. In the limit of large D this yields $w^2 \propto D$ or $w^2 \propto \ln D$ respectively for the case of short- or long-range forces between walls and the interface. We used the Nuclear Reaction Analysis depth profiling technique, to investigate this broadening effect directly in two binary polymer mixtures. Our results reveal that the interfacial width indeed increases with film thickness D, though the observed interfacial width is lower than the predicted w. This is probably due to surface tension effects imposed by the confining surfaces which are not taken into account in our model.

PACS. 68.10.m Fluid surfaces and fluid fluid interfaces – 68.15.+e Liquid thin films – 68.45.Gd Wetting

1 Introduction

Over the past several years processes of phase separation, wetting and dewetting in thin liquid films attracted attention in fields ranging from physics, and material science to the pharmaceutical industry and gave rise to a plenitude of theoretical [1–3], experimental [4–8] and Monte-Carlo simulation studies [9,10]. A binary (AB) mixture with an upper critical solution point T_c in the bulk will phase separate at $T < T_c$ into two coexisting phases with concentrations ϕ_1 and ϕ_2, respectively. In a thin film geometry with different boundary conditions at the air/film and film/substrate surfaces the interface between the two coexisting phases may be stabilized parallel to the substrate. This will occur whenever there is a sufficient preference of one of the confining surfaces for one of the phases.

In a pioneering theoretical work Parry and Evans [1] suggested that, in the temperature region between wetting temperature T_w and the bulk critical temperature T_{cb} of a binary mixture there should exist a kind of "soft mode phase". In this phase fluctuations along the phase 1/phase 2 interface are characterized by an anomalously large correlation length $\xi_\parallel$ for concentration fluctuations parallel to the confining walls of the thin film. According to their treatment the correlation length $\xi_\parallel$ of the fluctuations along this freely fluctuating interface, for the case of short-range forces between the walls and the molecules in the mixture is given by

$$\xi_\parallel = \xi_0 \exp(\kappa\, D/4) \tag{1}$$

where ξ_0 is a length of the order of the bulk correlation length ξ_b on the coexistence curve, D is the film thickness,

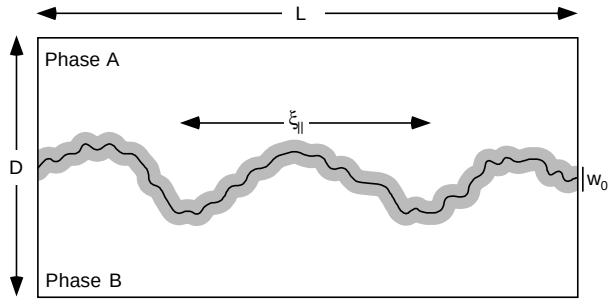

Fig. 1. Sketch of a cut through a thin phase-separated polymer film of lateral size L indicating the length scales relevant in our study. The interface (indicated in grey) between the two coexisting phases ϕ_1, ϕ_2 of an intrinsic width w_0 fluctuates around its mean position. The correlation length for fluctuations along this interface $\xi_\parallel$ scales according to the theory of Parry and Evans as $\xi_\parallel = \xi_0 e^{\kappa D/4}$ with the overall film thickness D.

[a] e-mail: bpklein@weizmann.weizmann.ac.il

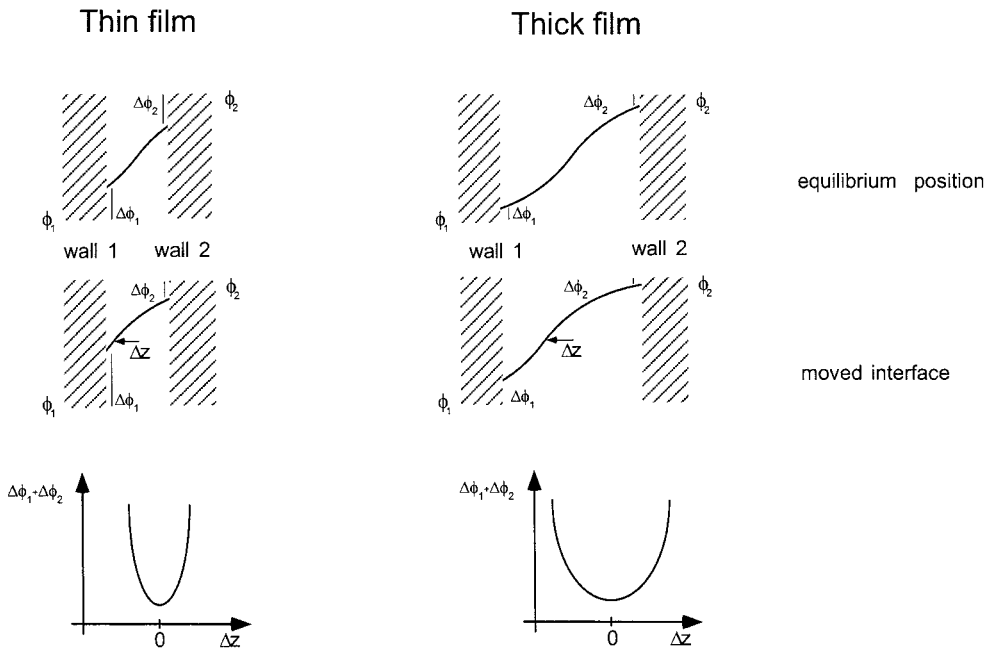

Fig. 2. Sketch of depth profiles through two different thick, phase separated samples. These profiles are commonly assumed to follow a tanh function as function of depth. The grey bars indicate the sample/air and sample/substrate interfaces, where the tanh profiles are cut off. The difference between the cut-off values of the profiles and the bulk coexisting values ϕ_1, ϕ_2 are labeled with $\Delta\phi_1$ and $\Delta\phi_2$ respectively. By moving the midpoint of the interface by a distance Δz from its equilibrium position the sum $\Delta\phi_1 + \Delta\phi_2$ increases. The comparison of the thin and thick film shows, that the sum increases faster for the case of thinner films.

and κ^{-1} is a transverse length scale. A sketch with the relevant length scales of the present study is shown in Figure 1. In the cases where mean field theory is valid [1] κ^{-1} can simply be set as ξ_b. In regions where it is no longer valid [11,12] κ^{-1} gets enhanced by fluctuations. The increase of fluctuations along the interface is demonstrated in the simple model shown in Figure 2. The sketch shows depth profiles $\phi(z)$ through two different, phase-separated samples of different thicknesses. According to Helfand and Tagami [13] and Binder [14] this profile is for the case of small spatial variations of $\phi(z)$:

$$\phi(z) = \frac{1}{2}\left\{(\phi_1 + \phi_2) + (\phi_1 - \phi_2)\tanh\left(\frac{z - z_0}{w_0}\right)\right\} \quad (2)$$

with ϕ_1, ϕ_2 being the coexisting values, z_0 the profile midpoint and w_0 the width of the interface. This profile approaches only exponentially the coexisting values for $z \to \pm\infty$. Due to the finite thickness of a film this interfacial profile is cut off before it reaches ϕ_1 or ϕ_2, respectively. As a result, one can model the effect of confinement by a parabolic potential for the deviation Δz of the interface from the midpoint position, as the following argument shows. In a gedankenexperiment we may move the profile midpoint by a finite distance Δz: $\phi(z') = \phi(z + \Delta z)$. One of the cut off values of the profile will now be closer to its coexisting value, but the second one will at the same time be further apart from its coexisting value. Since we are moving the interface away from the equilibrium position this movement will always cost energy – similar to a particle moving in parabola shaped potential. Comparing the case of a thin and a thick sample (Fig. 2) illustrates clearly, that in the case of the thinner sample the energy loss for a given Δz is bigger than in a thick sample. In terms of a particle in a parabolic potential this transfers to a much shallower potential for the thick film, or to larger fluctuations assuming a fixed exciting energy. Thus we qualitatively expect that the effective mean interfacial width, which is a convolution of the intrinsic width w_0 and the broadening due to capillary waves, will increase with increasing film thickness D. A brief report of this effect has appeared earlier [15].

In this paper we investigate this finite-size effect both experimentally and theoretically. In the following section we describe the experimental approach by which we measure directly the width of the interface between two coexisting phases of (polymeric) liquids in a thin film geometry. In Section 3 we review and develop the theory, making the arguments more precise and quantitative. In the following section our experimental results are compared with the theoretical predictions and in the final section we summarize and make some concluding remarks.

2 Experimental

2.1 Materials

The materials used for this study were random copolymers, in each of which the monomers have structure $(-C_4H_8-)$ and $(-C_2H_3(C_2H_5)-)$ randomly positioned along the chains. These polymers were made by hydrogenation or deuteration of the precursor unsaturated PBD chains as described in detail earlier [16,17]. Partial deuteration was necessary for labeling in the depth profiling method. The mean microstructure was $[(C_4H_8)_{1-x} - (C_2H_3(C_2H_5))_x]_N$ (henceforth designated hx when protonated and dx when deuterated, where x is in %). The dependence of the interfacial width between coexisting phases on the film thickness was studied from two different mixtures of polyolefins. System 1 was a mixture of $d75$ and $h66$ with an initial concentration of $\phi_{d75} = 0.60 \pm 0.01$,

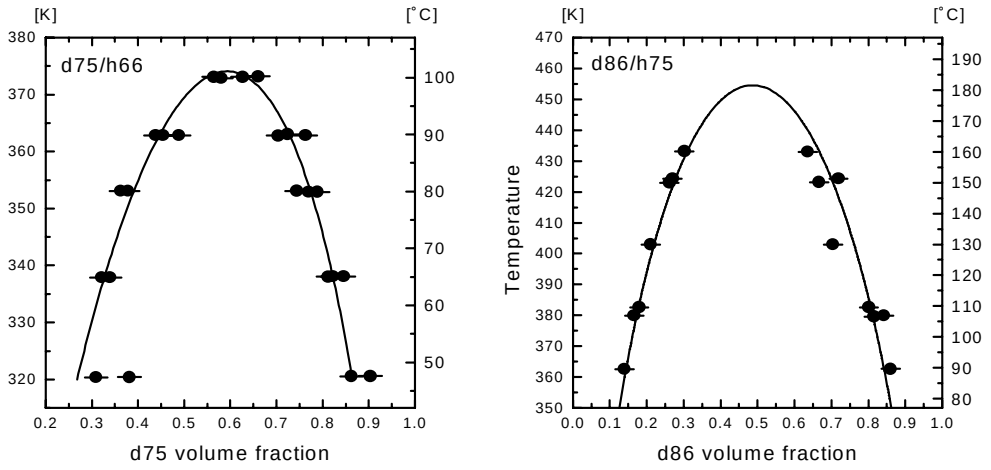

Fig. 3. Experimentally determined phase coexistence diagrams (binodals) of the blends $d75/h66$ and $d86/h75$, as determined by NRA [17]. From the binodal the bulk critical temperature for the $d75/h66$ blend is $T_{c,d75h66} = 101 \pm 4\,^{\circ}\mathrm{C}$ and $T_{c,d86h75} = 181 \pm 4\,^{\circ}\mathrm{C}$ for the $d86h75$ couple. The solid lines represent the best fits to the experimental data, calculated from the Flory-Huggins model with a ϕ-dependent interaction parameter $\chi(T,\phi) = (A/T + B)(1 + v\phi)$. The interaction parameters are $\chi_{d75h66} = (0.371/T - 2.7 \times 10^{-5})(1 + 0.212\phi)$ and $\chi_{d86h75} = (0.559/T + 8 \times 10^{-5})(1 - 0.057\phi)$, respectively.

system 2 consisted of $d86$ and $h75$ with an initial concentration of $\phi_{d86} = 0.50 \pm 0.01$. The degrees of polymerisation were $N_{86} = 1\,520$, $N_{75} = 1\,625$, and $N_{66} = 2\,066$. The polymers were in all cases highly monodisperse ($M_w/M_n < 1.08$). The bulk behaviour of both of the couples has been well characterized in earlier studies by Scheffold *et al.* [17,18]: bulk critical temperature, bulk critical volume fraction (of the deuterated component) and interaction parameter are $T_c = 181\,^{\circ}\mathrm{C}$, $\phi_c = 0.48$, and $\chi(T,\phi) = (0.559/T + 8 \times 10^{-5})(1 - 0.057\phi)$, for the case of the $d86/h75$ blend, and $T_c = 101\,^{\circ}\mathrm{C}$, $\phi_c = 0.61$, and $\chi(T,\phi) = (0.371/T - 2.7 \times 10^{-5})(1 + 0.212\phi)$, for the case of the $d75/h66$ blend. Phase coexistence curves (binodals) determined earlier [17] for these two mixtures are shown in Figure 3. Polished silicon wafers (P-type, $\langle 100 \rangle$ oriented, 6–13 Ω/cm obtained from the Institute of Electronic Materials Technology Warsaw) were used as supporting substrate for the polymer films. The toluene used was either Frutarum or Merck, analytical grade.

2.2 Sample preparation

Mixtures of above described couples were prepared in toluene with volume fractions of $\phi_{d86} = 0.50 \pm 0.01$ and $\phi_{d75} = 0.60 \pm 0.01$ for the $d86h75$ and $d75h66$ couples, respectively, and spin-cast from the solution onto gold covered silicon wafers to create films of uniform thickness in the range 150 to 1000 nm. By annealing these films under vacuum (5×10^{-3} Pa) at a temperature T_0 the films undergo phase demixing driving their compositions towards their coexisting values ϕ_1 and ϕ_2. The annealing temperature was $T_{0,d86h75} = 140\ ^{\circ}\mathrm{C}$ and $T_{0,d75h66} = 83\ ^{\circ}\mathrm{C}$, for the $d86h75$ and $d75h66$ couples, respectively. Annealing was carried out, until steady state was achieved. In all samples measured we found the resulting coexisting values (far from the interface) to agree within the scatter with the coexistence curves shown in Figure 3 After annealing the samples were quenched very rapidly to a temperature ($< -80\,^{\circ}\mathrm{C}$) below their glass transition temperature until measured.

2.3 Experimental technique

High resolution Nuclear Reaction Analysis (NRA) [19,20] was used to probe the depth-distribution profiles of the deuterated polymer chains. In this method a monoenergetic ^{3}He beam is incident at low angle α on the polymer sample, and undergoes the following reaction:

$$^3\mathrm{He} +^2 \mathrm{H} \rightarrow ^4 \mathrm{He} +^1 \mathrm{H} + Q,\ Q = 18.35\ \mathrm{MeV}. \quad (3)$$

From the energy spectrum of the emitted particles, the known energy losses, and reaction cross-section, the concentration profile $\phi(z)$ of the deuterated chains is directly measured, as function of depth. The spatial resolution of the method depends on the incident energy of the ^{3}He beam, the angle between beam and sample, on the depth within the sample, and on the particles being detected. It is highest at the sample surface. In these experiments we detect protons at a backward angle (proton-NRA), as can be seen in the sketch in Figure 4. The technique yields a spatial resolution of 4 nm HWHM at the polymer/air interface for an incoming ^{3}He energy of 700 keV and an angle of 8° between beam and sample, and stays better than approximately 25 nm HWHM for depths up to 600 nm for an incoming beam with energy 1.2 MeV under an angle of 14°. Figure 5 shows typical depth resolution profiles $\delta(D)$ of proton-NRA for different conditions of incident beam energy E and incident angle α. These resolution profiles were established by measuring single-component deuterated films of different thicknesses, spincast on gold-coated silicon wafers. Appropriate sets of conditions $\{E, \alpha\}$ were

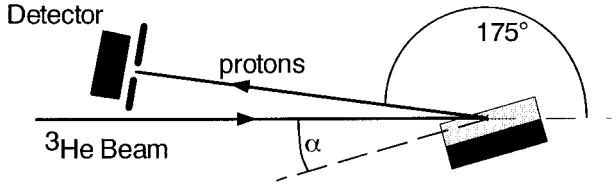

Fig. 4. The geometry of the proton-NRA setup used for depth profiling the polymer films. The use of proton-NRA enables us to achieve a resolution at the polymer / air surface of up to 4 nm HWHM; the angle α between beam and sample was typically in the range 4–14°.

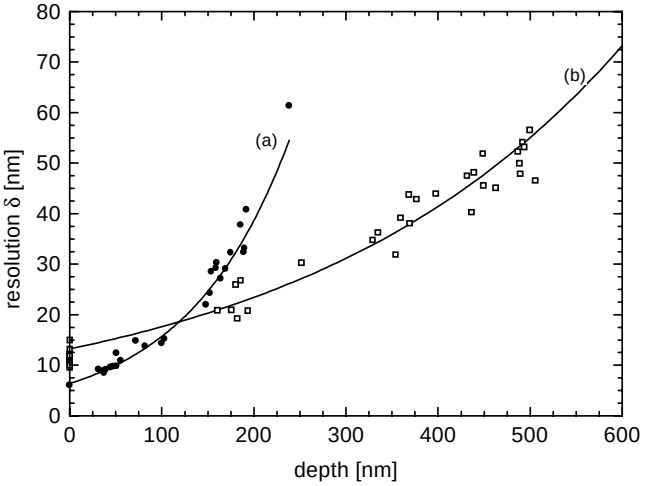

Fig. 5. Typical depth resolution profiles $\delta(D)$ of proton-NRA for different conditions of incident beam energy E and incident angle α. These resolution profiles were established by measuring single-component deuterated films of different thicknesses, spincast on gold-coated silicon wafers. The incident energies and angles were $E_{in,a} = 700$ keV, $E_{in,b} = 900$ keV, $\alpha_{in,a} = 8°$, and $\alpha_{in,b} = 14°$, for curves a and b, respectively.

subsequently used to measure the interfacial widths at different depths in the two-phase films, so as to optimize the high-resolution range. For each film of thickness D, a criterion of confidence in the profile of the interfacial region was that the resolution at the surface ($z = 0$) and that at the solid interface ($z = D$) should match that of $\delta(D)$ plot corresponding to the set of conditions $\{E, \alpha\}$ used. Moreover, several of the samples were profiled using two different sets of $\{E, \alpha\}$ giving always values for the interfacial width very close to each other.

Figure 6 shows two typical sets of depth profiles of phase separated samples with different overall film thicknesses. The dotted lines are the theoretical profiles

$$\phi(z) = \frac{1}{2}(\phi_1 + \phi_2 + (\phi_2 - \phi_1)\tanh\big((z - z_0)/w\big) \qquad (4)$$

which are cut off at $z = 0$ and $z = D$, where z_0 is the mean interface position. Since the experimental profiles are to some extent broadened by the system resolution $\delta(D)$ it is necessary to convolute the theoretical profiles with the independently determined depth-dependent resolution, resulting in the profiles drawn with solid lines. The profiles shown are the result of fits minimizing the deviation of the data points ϕ_i^{data} from the fitted curve ϕ_i^{fit}

$$dev = \sum_i \left(\phi_i^{fit} - \phi_i^{data}\right)^2. \qquad (5)$$

We used for our fitting program the Hooke and Jeeves non-linear optimization algorithm [21] in the implementation of Johnson [22]. As a further consistency check w was also determined in a number of cases by quadrature subtraction

$$w = \left[w_m(D)^2 - \delta(D_i)^2\right]^{1/2}. \qquad (6)$$

Here $w_m(D)$ is the measured width of the interface at depth D_i in a film of thickness D, obtained by fitting

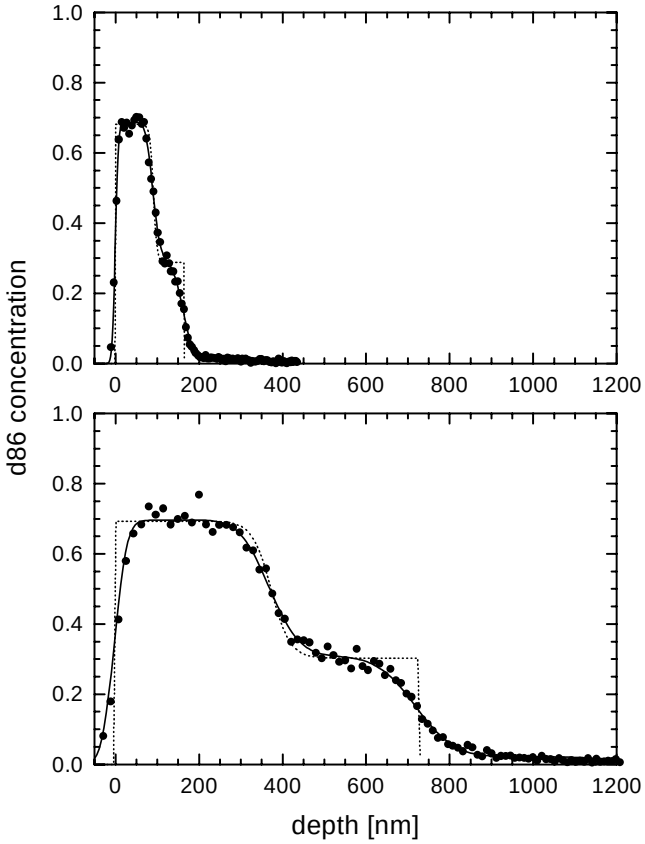

Fig. 6. Typical composition depth profiles of $d86/h75$ films annealed at $T_0 = 140\,^{\circ}$C. A $d86$ rich phase at the air interface (depth = 0) is coexisting with an d86 poor phase on top of an silicon wafer, as recorded by Nuclear Reaction Analysis (■). The dotted curves are the theoretical profiles $\phi(z) = 1/2(\phi_1 + \phi_2 + (\phi_2 - \phi_1)\tanh((z - z_0)/w)$, where z_0 is the midpoint of the interfaces between coexisting phases. The solid lines are the best fit to the data obtained by convoluting the theoretical profiles with the independently determined depth dependent resolution $\delta(z)$. The resolution corrected thicknesses of the shown profiles are $D_1 = 164$ nm and $D_2 = 728$ nm. A comparison of the two profiles shows already very clear the increase of the interfacial width with increasing overall film thickness. The resolution-corrected interfacial width $w = 8.5$ nm in the thinner film is significantly smaller than the interfacial width $w = 44.9$ nm of the thicker film.

to the as-measured profile, and $\delta(D)$ is the corresponding resolution at that depth. The values of w determined by these two approaches did always agree well with each other.

3 Theory

In this section we assume that the interfacial profile results from an "intrinsic" profile $\phi_A^{(int)}(z-z_0)$ that is broadened due to capillary waves, which lead to fluctuations of the local interface positions in the directions parallel to the confining walls. One describes this broadening by a convolution of the intrinsic profile $\phi_A^{(int)}(z-z_0)$ with a Gaussian distribution $P(z_0)$ due to capillary waves [23]

$$\begin{aligned}\phi(z) &= \int_{-D/2}^{D/2} dz_0 \phi^{(int)}(z-z_0)\, P(z_0) \\ &= \int_{-D/2}^{D/2} dz_0 \phi^{(int)}(z-z_0)\, \frac{1}{\sqrt{2\pi s^2}} e^{-z_0^2}/(2s^2). \end{aligned} \quad (7)$$

Here s^2 is the mean square width of the fluctuations of the midpoint position z_0 of the interface, *i.e.* $s^2 = \langle z_0^2 \rangle$ (note that we take the z-axis in the center of the thin films of thickness D, therefore $\langle z_0 \rangle = 0$). For simplicity, the intrinsic profile is approximated as an error function profile with the same slope as the tanh profile at $z = z_0$,

$$\begin{aligned}\phi^{(int)}(z) &= \frac{1}{2}\left\{(\phi_1+\phi_2) + (\phi_1-\phi_2)\tanh\left(\frac{z-z_0}{w_0}\right)\right\} \\ &\approx \frac{1}{2}\left\{(\phi_1+\phi_2) + (\phi_1-\phi_2)\,\mathrm{erf}\left(\frac{\sqrt{\pi}}{2}\,\frac{z-z_0}{w_0}\right)\right\}. \end{aligned} \quad (8)$$

This approximation describes the functional behaviour very well over the range of interest [24]. We now define the interfacial width w in terms of the maximum slope of the profile $\phi(z)$, which is also the operative experimental definition (Eq. (4))

$$w \equiv (\phi_2 - \phi_1) \Big/ \left[2\,\frac{d}{dz}\phi(z)\Big|_{z=0}\right]. \quad (9)$$

Using equation (8) in equation (7) we find for $D \to \infty$,

$$w^2 = w_0^2 + \frac{\pi}{2} s^2 \quad (10)$$

where w_0 is the intrinsic width of the interface. For polymer mixtures that are not too far away from the critical point T_c the intrinsic width of the interface is simply related to the bulk correlation length ξ_b, $w_0/2 = \xi_b$. In order to estimate s^2, we invoke the theory of Parry and Evans [1,11,25] who describe the confined interface within the "sharp-kink"-approximation in the "soft-mode" phase by the following Hamiltonian for the local interface position $z_0(x,y)$, namely the capillary wave Hamiltonian in a field due to the walls,

$$\begin{aligned}\frac{1}{k_b T} H_{eff}\{z_0(x,y)\} = \int dx\, dy \Bigg\{ &\frac{\sigma}{2}\left[\left(\frac{\partial z_0}{\partial x}\right)^2 + \left(\frac{\partial z_0}{\partial y}\right)^2\right] \\ &+ a_0 \left[\frac{T - T_c(D)}{T_w}\right] \kappa^2 z_0^2(x,y)\, e^{-\frac{\kappa D}{2}} \Bigg\}. \end{aligned} \quad (11)$$

Here k_b is Boltzmann's constant, T absolute temperature, $\sigma \equiv \Sigma/k_bT$ with Σ being the interfacial tension, and a_0/σ is a dimensionless constant of order unity. T_w is the wetting transition temperature that the model is expected to show for $D \to \infty$, while for finite D rather an interface delocalisation transition occurs for a critical temperature $T_c(D)$ slightly below T_w. The quadratic "potential" $V(z_0)$ (second term of Eq. (11)) actually results from expanding exponentially decaying potentials from the two walls, $V_{walls}(z_0) \propto \exp[-\kappa(D/2+z_0)] + \exp[-\kappa(D/2-z_0)]$, which "penalize" any fluctuations of the interface far away from its equilibrium position $z_0 = 0$. Thus, equation (11) presents a more quantitative origin of the parabolic potential anticipated in Figure 2. The decay constant $\kappa^{-1} = \xi_b$ in mean field [1] while more refined work has shown a fluctuation correction [12]

$$\kappa^{-1} = \xi_b(1+\omega/2), \qquad \omega = \left[4\pi\xi_b^2\sigma\right]^{-1}. \quad (12)$$

Equation (11) looks like the Landau-Ginzburg-Wilson Hamiltonian of phase transitions of a "spin field" $z_0(x,y)$ in two dimensions. From this analogy one can directly infer that (in a mean field treatment) the correlation $\xi_\parallel$ can be calculated as

$$\xi_\parallel^{-2} = \frac{1}{\sigma}\left(\partial^2 V(z_0)/\partial z_0^2\right)_{z_0=0} \quad (13)$$

which yields

$$\xi_\parallel = \kappa^{-1} e^{\kappa D/4} \sqrt{\frac{\sigma T_w}{2a_0\big(T - T_c(D)\big)}}. \quad (14)$$

Given the fact that the constant a_0 is not known for polymer mixtures, and that the square root factor in equation (14) presumably is of order unity (because the temperature T is not close to $T_C(D)$, which is near T_W), we shall in the following ignore this square root factor altogether and simply take $\xi_\parallel \approx \kappa^{-1}\exp(\kappa\, D/4)$. A computer simulation of polymer mixtures where $\xi_\parallel$ has been directly determined [25] supports that this is a reasonable approximation.

It now remains to calculate $s^2 = \langle z_0^2 \rangle$ from equation (11). First we note that if $V(z_0)$ could be neglected then we would have the simple capillary wave Hamiltonian $(1/k_bT)H_{cw}$. This is straightforwardly handled in reciprocal space and leads to the well-known logarithmically divergent integral,

$$s^2 = \frac{1}{2\pi\sigma}\int \frac{dq}{q} = \frac{1}{2\pi\sigma}\ln\left(\frac{q_{max}}{q_{min}}\right). \quad (15)$$

For a freely fluctuating interface (in the absence of fields such as gravity), one takes cutoffs for the momentum integration $q_{max} = 2\pi/\xi_b$, $q_{min} = 2\pi/L$, where L is the lateral linear dimension of the interface, to find (using also Eq. (10))

$$s^2 = \frac{1}{2\pi\sigma}\ln\left(\frac{L}{\xi_b}\right)$$
$$\left(\frac{w}{2}\right)^2 = \xi_b^2 + \frac{1}{16\sigma}\ln\left(\frac{L}{\xi_b}\right) = \xi_b^2\left[1 + \frac{1}{16\xi_b^2\sigma}\ln\left(\frac{L}{\xi_b}\right)\right]$$
$$= \xi_b^2\left[1 + \frac{\pi\omega}{4}\ln\left(\frac{L}{\xi_b}\right)\right] \quad (16)$$

where in the last step equation (12) was used. Equation (16) incorporates the well-known logarithmic divergence of the interfacial width with the lateral linear dimension of the system.

For a confined interface, however, where the full Hamiltonian (Eq. (11)) must be used, it clearly does not make sense to consider capillary waves of wavelengths larger than the correlation length $\xi_\parallel$, equation (14), as this is the largest length over which a correlation in $z_0(x, y)$ can persist. Basically the effect of the potential $V(z_0)$ in the calculation of s^2 is to provide a cut-off $q_{min} = 2\pi\xi_\parallel$ rather than $q_{min} = 2\pi/L$ (assuming that $L \gg \xi_\parallel$). Consequently we have from equation (15)

$$s^2 = \frac{1}{2\pi\sigma}\ln\left(\frac{\xi_\parallel}{\xi_b}\right) = \frac{1}{2\pi\sigma}\left[(\kappa D/4) - \ln(\kappa\xi_b)\right] \approx \frac{\kappa D}{8\pi\sigma} \quad (17)$$

and equation (10) then yields, using again equation (12)

$$w^2 = 4\xi_b^2 + \frac{\kappa D}{16\sigma} = 4\xi_b^2 + \pi\omega\xi_b^2\frac{\kappa D}{4}$$
$$= 4\xi_b^2 + \frac{\pi\omega}{1+\omega/2}\frac{\xi_b D}{4}. \quad (18)$$

We now turn to the estimation of the constant ω. For the polymer mixture $d75h66$ we estimate $\xi_b \approx 18.8$ nm (see next section) [26]. In order to estimate σ we simply take the formula for symmetrical polymer mixtures [14]

$$\sigma \approx \frac{2}{3b^2\sqrt{N}}\left(1 - \chi_{crit}/\chi\right)^{3/2} \quad (19)$$

valid in mean field theory, using $b \approx 0.64$ nm and $(1 - \chi_{crit}/\chi) \approx (1 - T/T_{cb}) \approx 0.0481$ at the temperature of the experiment [15]. This yields (taking for N the geometric mean of both chain lengths $N_A = 1\,625$, $N_B = 2\,030$) $\omega \approx 0.558$, and the numerical factor in equation (18) $\pi\omega/(1+\omega/2) \approx 1.37$. In our preliminary communication [15], this factor was simply put to unity. In view of the fact that σ is not independently known and equation (19) is probably a rather crude approximation, and also ξ_b is known only somewhat imprecisely, the precise estimation of this factor is a problem. We note that this factor is temperature dependent, since ω is strongly temperature dependent in the mean field critical regime [27]

$$\omega_{MF} = \omega_0\left(1 - \chi_{crit}/\chi\right)^{-1/2} \quad (20)$$

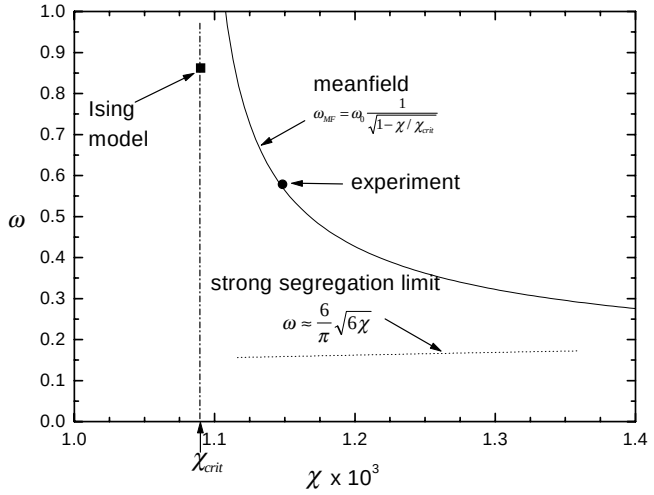

Fig. 7. Capillary parameter ω as function of the interaction parameter χ for the case of the $d75h66$ mixture. Close to χ_{crit} we expect a crossover from the mean field behaviour $\omega_{MF} = \omega_0(1-\chi/\chi_{crit})^{-1/2}$ to the Ising critical universal value $\omega_{Ising} \approx 0.86$. For larger χ, another crossover occurs towards the case of strongly segregated interfaces. The error of the shown curve (and thus also of the point marked "experiment") is mostly due to uncertainty in the critical surface tension, for which we have taken the mean field result for a symmetrical polymer mixture. We estimated this error is of the order of several percent.

and the prefactor ω_0 for symmetrical polymer mixtures is expected to scale with the chain length N as $\omega_0 \propto 1/\sqrt{N}$ [27]. However, very close to χ_{crit}, namely for $N(1 - \chi_{crit}/\chi) \ll 1$, we expect a crossover to the Ising critical universal value $\omega_{Ising} \approx 0.86$ [28], see Figure 7. For larger χ, another crossover occurs towards the case of strongly segregated interfaces, where one can infer from the theory of Helfand *et al.* [13,29] that $\omega \approx 6\sqrt{6\chi}/\pi$. For the additional system $d86/h75$ studied in the present paper we find $\omega \approx 0.360$ rather than $\omega = 0.460$, and $\pi\omega/(1+\omega/2) \approx 0.958$, if ξ_b is estimated as $\xi_b = 12.8$ nm.

It should be stressed that the above treatment implies that the surface-monomer interaction is of short range: only then one finds an effective potential for an interface at a distance l from the wall of the form $V(l) \propto \exp(-\kappa l)$. Van der Waals interactions, however, would lead to a power-law potential $V(l) \propto l^{-p}$ where p is some exponent — some support for this has been provided by a recent study of of wetting dynamics in similar polymer mixtures [30] and by neutron reflectrometry measurements of a polymer mixture in the strong segregation limit [31]. In equation (11) this would mean that the term $e^{-\kappa D/2}$ is replaced by a term proportional to D^{-p}, and the correlation length $\xi_\parallel$ gets a prefactor proportional to $D^{(p/2+1)}$ instead of $\exp(\kappa D/4)$. This would lead to a significantly weaker increase of the interfacial width ($\omega^2 \propto (p/2+1)\ln(D)$ rather than $\omega^2 \propto D$). Working out a formula analogous to equation (18) for this long-range potential for the case $p = 3$ yields

$$w^2 = 4\xi_b^2 + \frac{5\pi}{2}\xi_b^2\omega\ln\left(\frac{D}{2\xi_b}\right). \quad (21)$$

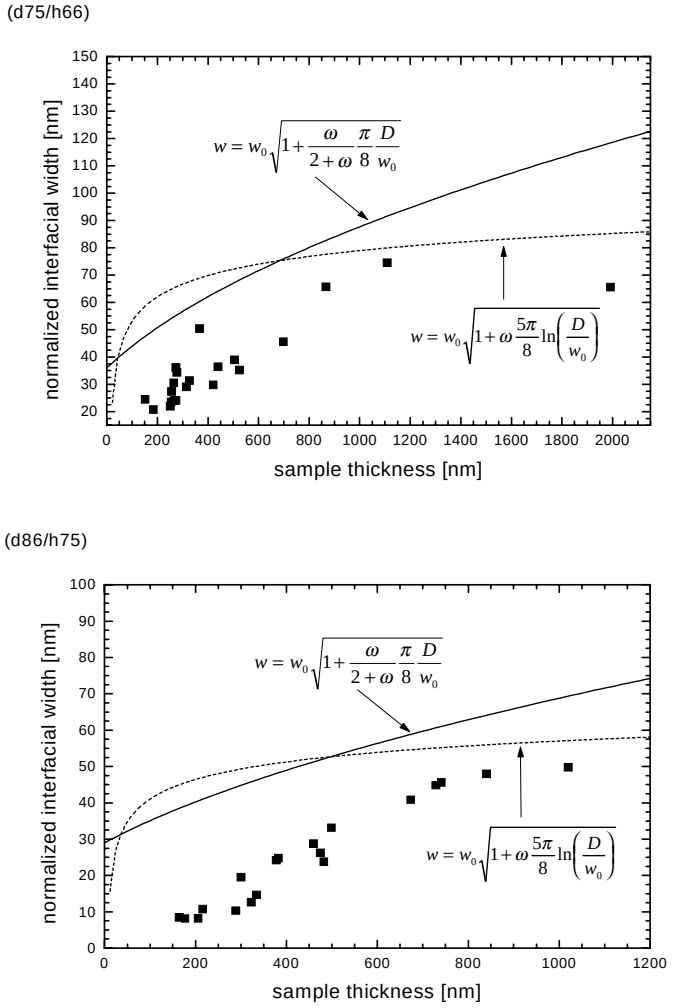

Fig. 8. Plot of the interfacial width w against the sample thickness D for the two blend s of the olefinic copolymers $d76h66$ (a) and $d86h75$ (b) as described in the text, extracted from profiles such as shown in Figure 6. The full lines show equation (18) and the broken lines show equation (21), using for the capillary parameter $\omega_{d75h66} = 0.558$ and $\omega_{d86h75} = 0.360$.

4 Results

In Figure 6 typical composition depth profiles of two annealed $d86/h75$ films with thicknesses (a) $D_1 = 164$ nm and (b) $D_2 = 728$ nm can be seen. A comparison of the two profiles shows already very clearly the increase of the interfacial width with increasing overall film thickness. The resolution-corrected interfacial width $w = 8.5$ nm (a) in the thinner film is significantly smaller than the interfacial width $w = 44.9$ nm (b) of the thicker film.

Figure 8 summarizes the data over the entire D range studied for both couples together with the theoretically predicted curves equation (18) (solid line) and equation (21) (dashed line). The values used for ξ_b and ω were calculated according to the formulas valid for symmetric polymer blends, and are summarized in Table 1. However, as is shown in Table 1, the values obtained by applying the theory for asymmetric polymer blends [14], are quite comparable. The theoretical prediction of equation (18) describes the qualitative behaviour of the data very well and correctly predicts the order of magnitude of the effect. In the limit of D comparable to ξ_b the model calculations [25] predict a behaviour of $w \propto D$, (see also next section) which also can be seen in the experimental data in the range of D between 150 and 750 nm. However, the range of this approximately linear variation, namely up to $D \approx 750$ nm $\approx 22w_0$, is much larger than expected, indicating that neither functional form, equation (18), or equation (21) is very close. A point of interest is that although the main qualitative feature, that the interfacial width increases with D, is clearly observed, the actual values are in all cases lower than the predicted ones. We relate to this in more detail in the next section.

This large range of linear variation of w *vs.* D is somewhat larger than suggested in a recent Monte-Carlo study of the bond fluctuation model of symmetric polymer mixtures [25]. For the sake of comparison, we reproduce some of those data here (Fig. 9). This calculation refers to a chain length $N_A = N_B = N = 32$, and as Figure 9a shows, the segregation of the pure phases is complete at the temperature chosen in the simulation ($\phi_1 = 0$, $\phi_2 = 1$), unlike the experiment. Calculating the intrinsic width from the self-consistent field theory as $w_0 = 4.65$ lattice spacings, and using the interfacial tension $\sigma = 0.015$ as found from an independent simulation [25] (choosing the lattice spacing as the unit of length), equation (18) can be worked out without any adjustable parameters. We find that it agrees with the simulation data for $D \geq 45$ lattice spacings (Fig. 9b), *i.e.* the regime of the initially stronger linear variation $w \propto D$ in the simulation ends at $D \approx 10w_0$ already, whereas in the experiments it appears to be around double that value.

In addition, we see in Figure 8 that the experimentally determined interfacial width appears to saturate (*i.e.* to become independent of D) for film thicknesses above 750 nm. The reason for this is, we believe, due to the fact that the parallel correlation lengths becomes comparable with the lateral dimensions of our samples. According to classical capillary wave theory the lateral sample size L_{max} provides a further fixed upper cut-off for the spectrum of capillary wave excitations (as earlier discussed). This implies that from the point where $L_{max} < \xi_{\|}(D)$ we cannot expect a further increase of the interfacial width with increasing film thickness, as can indeed be seen in our experimental data (Fig. 8, at $D \geq 800$ nm). In practice we might expect L_{max} to take the value not of the sample size (*ca.* 1 cm) but rather of the beam cross-section at the sample, which is somewhat smaller, of order of millimeters. Additional constraints arise at the lower D limit when the films have thicknesses in the order of a chain coil size. Clearly as the film becomes of thickness comparable to ξ_b, it becomes meaningless to talk of interfacial widths of this magnitude. Since this has not been taken into account for the model, we expect further deviations for the case of film thicknesses $D \to 0$.

Table 1. Degree of polymerization N of the polymers used, critical temperatures T_{cb} and concentrations ϕ_{crit} of the two blends and coordinates in phase space (T, ϕ_1, ϕ_2), where the measurements were preformed, as well as the average statistical segment length b. From these values we calculated the bulk correlation length ξ_b according to $\xi_b = (b/6)/\sqrt{\frac{1-\phi}{2N_A} + \frac{\phi}{2N_B} - \chi_{SANS}(\phi)\,\phi\,(1-\phi)}$, using $\chi(\phi,T) = \chi_0(T)(1+A\phi)$ and $\chi_{SANS}(\phi,T) = \chi_0(T)(1-A+3A\phi)$, where $A_{d75h66} = 0.212$ and $A_{d86h75} = -0.057$ for the $d75h66$ and the $d86h75$, respectively. This yields the values for the intrinsic interfacial width $w_0 = \xi_{b,1} + \xi_{b,2}$ and the parameter ω. For a comparison we give additionally the values for ξ and ω, calculated with the formula for symmetric blends: $\xi_{sym} = (b/6)(N_A N_B)^{1/4}(1-\chi_{crit}/\chi)^{-1/2} \approx (b/6)(N_A N_B)^{1/4}(1-T/T_c)^{-1/2}$, and $\omega_{sym} = \left[2\pi (N_A N_B)^{1/4}(1-T/T_c)^{1/2}/27\right]^{-1}$.

system	N_A	N_B	T_{cb} (°C)	T (°C)	ϕ_{crit}	ϕ_1	ϕ_2
$d75/h66$	1 625	2 030	101	83	0.61	0.39	0.77
$d86/h75$	1 520	1 625	181	140	0.48	0.24	0.73
system	b (Å)	$\xi_{b,1}$ (nm)	$\xi_{b,2}$ (nm)	w_0 (nm)	ω	ξ_{sym} (nm)	ω_{sym}
d75/h66	6.4	18.4	19.2	37.6	0.558	20.7	0.460
d86/h75	5.8	12.7	12.9	25.6	0.360	12.8	0.360

5 Summary, discussion and conclusions

The present study reveals two main findings, underpinned both by experiments and by theoretical and simulation work. The first is that in a phase-separated sample in a film of finite thickness D, where the inter-phase boundary is parallel to the film, the width w of the interface is broadened, due to capillary waves, to an extent which depends on D. The qualitative reason for this film-thickness dependence is as follows: larger excursions of the mean interface position bring it closer to the confining surfaces, and these cut off the interface profile thereby costing energy. A given excursion thus costs less energy in a thicker film, and hence thicker films are associated with larger values of w. More quantitatively, one considers that the capillary waves lead to fluctuations of the local interface positions in the direction parallel to the confining walls. For short range forces between the walls and the molecules of the mixture, the correlation length $\xi_\parallel$ for these concentration fluctuations varies exponentially with D, $\xi_\parallel = \xi_b \exp(\kappa D/4)$. This correlation length may be considered as an upper cut-off for the spectrum of capillary waves on this interface (that is, as the effective maximum lateral dimension of the capillary-broadened interface). Together with the classical result that the mean square width of an interface broadened by capillary waves increases as the logarithm of its lateral dimension, this leads to a film thickness dependence of the interfacial width. A more detailed theoretical treatment gives precise predictions. According to this argument, the "intrinsic" interfacial profile width w_0 (as predicted by mean field theory, for instance) is not directly observable, but is convoluted with the capillary broadening to yield w. We demonstrated by direct depth profiling of thin phase separated polymer films that this kind of effect indeed exists. This confirms experimentally a new type of finite-size effect for the structure of interfaces in layered phases. It is of interest that for sufficiently thick films w appears to saturate, as would indeed be expected whenever $\xi_\parallel$ exceeds the macroscopic lateral dimension of the sample (or, as in this case, the lateral dimension, of order millimeters, of the experimental depth profile probe).

Our second main finding is that the magnitude of the measured interfacial width is less than expected over the entire range of the film thickness D. Both equations (18, 21), describing the interfacial broadening for short-range or for long-range wall-molecule forces respectively, are valid only asymptotically in the limit of very thick films, $D \gg w_0$, where w_0 is the intrinsic interfacial width. In this limit our model predicts $w^2 \propto D$. It is clear that for ultra-thin films (where $D < w_0$) the observed interfacial width can never exceed the film thickness, and hence one must have $w \propto D$ for very thin films. In practice, the range of D over which this linear variation is roughly true is surprisingly large. The simulations (Fig. 9) suggest that the quasi-linear regime extends up to $D \approx 10 w_0$, while the experiments (with admittedly more scatter) show that an approximately linear variation would be consistent with the data even for thicknesses up to $D \approx 20 w_0$ or so. In addition to the obvious effect noted above, arising when the film thickness values are of order of the interfacial width itself, there is an additional factor which may contribute to the origin of such an effect, which was not taken into account in our calculations. This is the higher surface tension associated with variation of the composition profile as the interface excursions approach a confining surface: since each surface "selects" the pure phase with which it prefers to be in contact (thereby also leading to the layering parallel to the surfaces), any deviation from the pure phase composition must lead to increase in the surface energy. This additional factor would have the effect of suppressing the broadening of the interface even further, and making the measured width less than that predicted, as observed.

It is also of interest to compare in more detail the theoretical predictions and simulations with the experimental results. With respect to the extent of broadening, where the observed effects are less than predicted, there are a number of conceivable reasons why the effect of the walls in the experiment is stronger than in the simulation.

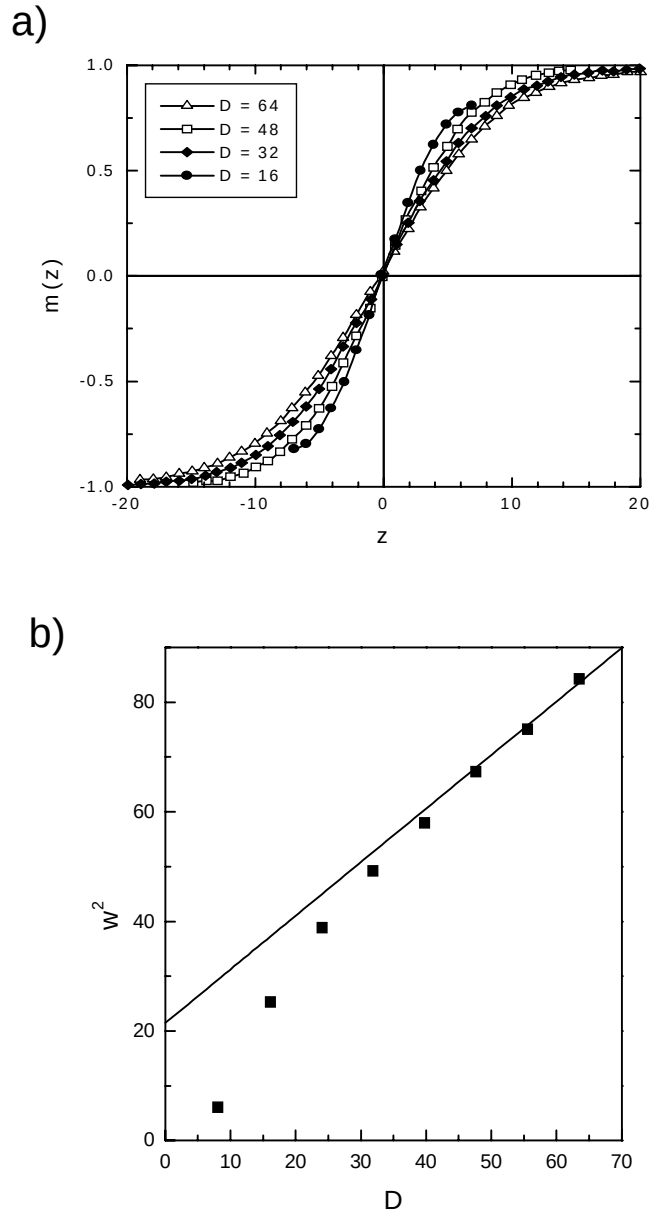

Fig. 9. (a) Order parameter profiles $m(z) = \big(\phi_A(z) - \phi_B(z)\big)/\big(\phi_A(z) + \phi_B(z)\big)$ plotted *vs.* $z - D/2$, for films of the thickness $D = 16$, 32, 48 and 64 lattice spacings, walls being situated at $z = 0$ and $z = D$. Data points are Monte-Carlo results for a symmetric polymer mixture, chain length $N = 32$, $T/T_c = 0.48$. (b) Squared interfacial width w^2 *vs.* D for a lateral size $L = 256$. The straight line shows equation (18) (from Werner *et al.* [25]).

(i) The latter considers the strong segregation limit, and rather short chains, the walls are perfectly flat and they are precisely "anti-symmetric" (*i.e.*, the strength of the wall potential attracting A-monomers on one side is exactly the same as the strength of the wall potential attracting B-monomers on the other side). Clearly such a model is too idealized to describe the present experiments, where the polymer/air and polymer/solid surfaces are neither ideally smooth nor symmetric in their potential.

(ii) The actual potential due to external boundaries on a confined interface most probably is a combination of strong short range forces and weaker long range van der Waals forces. Direct evidence for this has come from studies of both wetting dynamics in thin films [30], and of interfacial structure [31]. It is not known how such forces affect even the "intrinsic" thickness w_0 of the interface. In recent simulation work for short range forces [25,32] it was shown that the effective interfacial tension $\sigma(l)$ of an interface at a distance l from a wall gets more enhanced at smaller l, which leads to a corresponding reduction of w_0.

(iii) The parameters ξ_b, σ (and subsequently $\omega = (4\pi\xi_b^2\sigma)^{-1}$) needed in equations (18, 21) are known only to within some uncertainty (see *e.g.* values of ξ_b estimated using different approaches, in Tab. 1). In addition, all these formulas are of a mean field character and break down as $T \to T_c$. Since our systems are studied at about 9% or 5% below T_c, the crossover to the Ising model critical behaviour could affect some of these estimates. This problem seems to be particularly severe for the parameter ω, Figure 7, which approaches $\omega_{crit} \approx 0.86$ at T_c (this is believed to hold universally for all binary mixtures including polymers), while our estimates for ω are smaller (note that the strong segregation limit in Figure 7 presumably is a lower bound on ω). Theoretical work would be desirable to describe the temperature dependence of ω for polymers more fully.

(iv) Since the length scale $\xi_{\|}$ for large D becomes very large, limitations due to the finite lateral extent of the sample, as well as the question whether the annealing time suffices to equilibrate long wave length fluctuations on these large scales, may be a problem as well.

Despite these limitations, the theory is able to predict the existence of the anomalous size-dependence of the interfacial profile and its width qualitatively, and roughly estimate the order of magnitude of the effect. Our experimental data give clear evidence (Fig. 8) that under typical conditions this effect is not small (w varies by a factor of 2 or 3 when D changes from 100 to 1000 nm) and there is no clear way whereby the "intrinsic width" w_0 could be read off from such data. Thus the idea [33] that one can use experiments of interfacial profiles in thin film geometry to estimate the χ parameter of blends using theoretical formulas for the intrinsic width w_0 seems to be problematic.

Finally, we recall earlier studies of interfacial widths between coexisting polymer phases in thin films, where the capillary broadening effect was not considered [34–36]. These were mostly carried out for film thicknesses in the range $D = 500$–600 nm, where — as seen in the present study — the interfacial widths w (Fig. 6) are comparable, or somewhat larger than the intrinsic widths w_0. As a result of this study, and of the above discussion, the origin of this is now clearer. It is of interest that the observed interfacial widths in these earlier [34–36] were indeed somewhat larger in all cases than the mean field values w_0.

We are grateful to A. Werner for allowing us to reproduce the present Figures 7a, 7b from reference [25], and thank him as

well as M. Müller and F. Schmid for helpful and stimulating discussions. We particularly appreciate the careful reading of the manuscript and the thoughtful comments by A. Budkowski. This work was supported by the German-Israeli-Foundation (GIF) under contract I-0438-145-07/95 (K.B.), by the Minerva Center for Supermolecular Architecture at the Weizmann Institute, the Israel Science Foundation, the Ministry of Arts and Sciences (Tashtit programme).

References

1. A.O. Parry, R. Evans, Physica A **181**, 250 (1992).
2. J.F. Joanny, Phys. Chem. Hydrodun. **9**, 183 (1987).
3. F. Brochard-Wyart, P. Martin, C. Redon, Langmuir **9**, 3682 (1993).
4. U. Steiner, J. Klein, L.J. Fetters, Phys. Rev. Lett. **72**, 1498 (1994).
5. U. Steiner, J. Klein, E. Eiser, A. Budkowski, L.J. Fetters, Science **258**, 1126 (1992).
6. R.A.L. Jones, Polymer **35**, 2160 (1994).
7. W. Straub, F. Bruder, R. Brenn, G. Krausch, H. Bielefeldt, A. Kirsch, O. Marti, J. Mlynek, J.F. Marko, Europhys. Lett. **29**, 353 (1995).
8. R. Yerushalmi-Rozen, K. Klein, J. Phys.-Cond. **9**, 7753 (1997).
9. K. Binder, D.P. Landau, A.M. Ferrenberg, Phys. Rev. E **51**, 2823 (1995).
10. A.K. Chakraborty, D. Bratko, J. Chem. Phys. **108**, 1676 (1998).
11. K. Binder, R. Evans, D.P. Landau, A.M. Ferrenberg, Phys. Rev. E **53**, 5023 (1996).
12. C.J. Boulter, A.O. Parry, Phys. Rev. Lett. **74**, 3403 (1995).
13. E. Helfand, Y. Tagami, J. Chem. Phys. **57**, 1812 (1972).
14. K. Binder, J. Chem. Phys. **79**, 6387 (1983).
15. T. Kerle, J. Klein, K. Binder, Phys. Rev. Lett. **77**, 1318 (1996).
16. N.P. Balsara, L.J. Fetters, N. Hadjichristides, D.J. Lohse, C.C. Han, W.W. Graessley, R. Krishnamorti, Macromol. **25**, 6137 (1992).
17. F. Scheffold, E. Eiser, A. Budkowski, U. Steiner, J. Klein, L.J. Fetters, J. Chem. Phys. **104**, 8786 (1996).
18. F. Scheffold, A. Budkowski, U. Steiner, E. Eiser, J. Klein, L.J. Fetters, J. Chem Phys. **104**, 8795 (1996).
19. T. Kerle, F. Scheffold, A. Losch, U. Steiner, G. Schatz, J. Klein, Acta Polymerica **48**, 548 (1997).
20. U.K. Chaturvedi, U. Steiner, O. Zak, G. Krausch, G. Schatz, J. Klein, Appl. Phys. Lett. **56**, 1228 (1990).
21. R. Hooke, T.A. Reeves, J. ACM **8**, 212 (1961).
22. M.G. Johnson, `http://www.netlib.org` (1994).
23. D. Jasnow, Rep. Prog. Phys. **47**, 1059 (1984).
24. A. Losch, R. Salomonovic, U. Steiner, L.J. Fetters, J. Klein, J. Polym. Sci. **33** (1995).
25. A. Werner, M. Müller, F. Schmid, K. Binder, J. Chem. Phys. **107**, 8175 (1997).
26. In our earlier communication this value was inadvertently given in error as 10.6 nm.
27. I. Schmidt, K. Binder, J. Phys. France **46**, 1631 (1985).
28. M.E. Fisher, H. Wen, Phys. Rev. Lett. **68**, 3654 (1992).
29. E. Helfand, Y. Tagami, J. Chem. Phys. **56**, 3592 (1971).
30. U. Steiner, J. Klein, Phys. Rev. Lett. **77**, 2526 (1996).
31. M. Sferrazza, C. Xiao, R.A.L. Jones, D.G. Bucknall, J. Webster, J. Penfold, Phys. Rev. Lett. **78**, 3693 (1997).
32. M. Müller, K. Binder, Macromol. (submitted, 1997).
33. M. Stamm, D.W. Schubert, Ann. Rev. Mater. Sci. **25**, 326 (1995); M. Stamm, Macromol. Symp. **112**, 25 (1996).
34. U. Steiner, G. Krausch, G. Schatz, J. Klein, Phys. Rev. Lett. **64**, 1119 (1990).
35. U.K. Chaturvedi, U. Steiner, O. Zak, G. Krausch, Phys. Rev. Lett. **63**, 616 (1989).
36. E. Eiser, A. Budkowski, U. Steiner, J. Klein, L.J. Fetters, R. Krishnamoorti, PMSE Proceedings, Am. Chem. Soc. **69**, 176 (1993).